

# Short Range Order and Stability of a Mechanically Alloyed Cr<sub>25</sub>Nb<sub>75</sub> Glass Determined by Total Scattering and First Principles

Georgios S.E. Antipas\*

School of Mining Engineering and Metallurgy, National Technical University of Athens,  
Zografou Campus, Athens 15780, Greece

Received: September 2, 2014; Revised: October 25, 2014

The atomic environment and stability of an amorphous Cr<sub>25</sub>Nb<sub>75</sub> alloy was studied on the basis of average atomic coordination, average cluster number density as well as cluster radial distribution of these quantities based on Reverse Monte Carlo fitting of multiple total scattering datasets. A number of the most representative clusters of the RMC supercell were isolated and relaxed via Density Functional Theory. Average coordination of both Cr and Nb atoms was similar, possibly due to the similarity of their covalent radii. Also, the histograms of average coordination of both species suggested binomial distributions, possibly reflecting two separate modes of atomic bonding. Cr-centered clusters were found to be more cohesive than Nb-centered ones and overall cluster stability appeared to be correlated to minority Cr valence populations.

**Keywords:** Cr-Nb glass, short range order, electronic structure, Reverse Monte Carlo, density functional theory

## 1. Introduction

The Cr-Nb matrix is of frequent reference in anti-corrosive and glass forming applications<sup>1</sup>. Cr-Nb has also been associated with the facility to create the basis of solid solutions via mechanical alloying such as high-energy ball milling<sup>2</sup> and both ends of the Cr-Nb phase diagram have been investigated to that extent. For instance, in the Cr end (Cr<sub>67</sub>Nb<sub>33</sub>) the formation of a metastable bcc phase has been achieved by mechanical alloying<sup>3</sup>, yielding a periodic structure which involved the presence of the Cr<sub>2</sub>Nb intermetallic. Typically, alloys which contain Cr<sub>2</sub>Nb are candidates for high-temperature structural applications<sup>4</sup> which require oxidation resistance<sup>5</sup> and for compositions up to approximately 37 at.% Nb, Cr<sub>2</sub>Nb is naturally derived as it is the only stable phase in the Cr-Nb phase diagram, crystallizing either into the cubic or the hexagonal lattice. However, the Nb-rich end of the Cr-Nb phase diagram may lead to both crystalline and amorphous phases, the structure of the latter mostly unexplored. For example, the possibility of formation of crystalline and amorphous structures by ball milling in the Nb end of the phase diagram has been investigated<sup>6</sup> and in that work, formation of an amorphous phase from a Cr<sub>x</sub>Nb<sub>1-x</sub> ideal solution with x up to 80 at.% was flagged as possibility, on the basis of activation energies of the order of 0.03 eV; activation energies were calculated via a thermodynamic model which took into account grain growth, grain boundary migration and nucleation of new phases. Model predictions were confirmed by the synthesis of a Cr<sub>25</sub>Nb<sub>75</sub> amorphous compound via mechanical alloying.

The atomic topology of a Cr<sub>25</sub>Nb<sub>75</sub> compound produced in<sup>6</sup> was determined by Reverse Monte Carlo (RMC) fitting of the experimental structure factor derived from the X-ray

diffraction (XRD) dataset. This enabled the determination of partial pair distribution functions and the extraction of the local atomic order in these glasses. As the RMC supercell is intractable quantum mechanically due to its size, here we have employed the facility of selecting clusters on the basis of the radial distribution of coordination features; the latter constitutes a novel and subtlety which we have presented previously<sup>7,8</sup>. We, hence, utilize this facility in order to use the local atomic order of the Cr<sub>25</sub>Nb<sub>75</sub> glass towards a discussion of the system's electronic structure and stability.

## 2. Methodology

The reference system of this study was a Cr<sub>25</sub>Nb<sub>75</sub> glass synthesized by ball milling in the work of Lima et al.<sup>6</sup>. For the sake of completeness we note that the process involved sealing a mixture of high-purity Cr and Nb powders (both powder particle sizes < 10 μm) in a cylindrical steel vial together with several steel balls (maintaining a ball-to-powder weight ratio of 6:1), under an argon blanket. Selected ball milling durations were 10, 25, 41 and 53 h and the steel vial was kept at ambient temperature by continuous ventilation. The resulting powders were analyzed via XRD at a Cu-K<sub>α</sub> wavelength. Analysis of the as-milled powder after 53 h of milling was done by energy dispersive X-rays analysis and revealed Cr and Nb contents of 25 at.% and 75 at.%, respectively. The material's structure factor was computed from the XRD pattern after corrections for polarization, absorption, and inelastic scattering. The number density and density of the amorphous alloy were calculated as 0.0516 atoms/Å<sup>3</sup> and 7.1 g/ml, respectively<sup>6</sup>. The experimental structure factor was fitted via a molecular RMC simulation of a supercell of 5000 atoms.

\*e-mail: [gantipas@metal.ntua.gr](mailto:gantipas@metal.ntua.gr)

Here, a number of Cr-, and Nb-centered clusters were selected as indicative of various sites within the RMC supercell of<sup>6</sup>, on the basis of the radial distribution of atomic environment statistics. Selected clusters were relaxed within the premise of Density Functional Theory (DFT) and were further analysed for molecular orbital interactions-induced stability. Spin unrestricted DFT relaxation was carried out within the scope of the Generalized Gradient Approximation (GGA) by use of a combination of the Becke exchange functional (B) and the Lee-Young-Parr correlation functional (LYP)<sup>9,10</sup>. Single-electron wavefunctions were expanded into uncontracted Slater-type orbitals (STO) comprising a triple- $\zeta$  (TZ) basis set with two sets of polarization functions (2P). Henceforth, the level of theory will be referred to as BLYP/TZ2P. Calculations were all-electron for both the Cr ([Ar]3d<sup>5</sup>4s<sup>1</sup>), and Nb ([Kr]4d<sup>4</sup>5s<sup>1</sup>) atomic structures, corrected for relativistic effects using the zero-order regular approximation (ZORA)<sup>11-13</sup>; the latter is a requirement raised by the presence of Nb. Relaxation simulations were followed by single point and frequency calculations for all structures to ensure full self-consistent field (SCF) convergence; however, some non-aufbau occupations did occur and these simulations were discarded. All DFT calculations were performed with the Amsterdam density functional (ADF) program<sup>14</sup>.

Clusters isolated from the RMC supercell do not correspond to any particular level of theory; they, hence, had to initially be relaxed into the BLYP/TZ2P level. Based on our previous studies of non-ferrous amorphous cluster relaxation<sup>7,8,15</sup>, we deemed that relaxation of the metal center while keeping the first coordination neighbours frozen was sufficient and it also provided good  $g(r)$  agreement with the un-relaxed geometries, both for charged and charge-neutral clusters. Hence, all results shown henceforth are based on DFT relaxed centers within frozen nearest neighbours, inclusive of the second coordination shell.

### 3. Results and Discussion

#### 3.1. Pair distribution functions and average coordination

The partial pair distribution functions,  $g(r)$ , on the basis of the RMC supercell are shown in Figure 1, while for a more comprehensive assessment of the quality of the RMC solution, the reader is referred to the paper by Lima et al.<sup>6</sup>. Principal short-range ordering was owing to a combination of Nb–Nb and Cr–Nb interactions, as indicated by the presence of both partials in the first coordination shell. As mentioned in the work by Lima et al.<sup>6</sup>, the average interatomic distances estimated by RMC were:  $r_{\text{Cr-Cr}} = 2.88 \text{ \AA}$ ,  $r_{\text{Cr-Nb}} = 2.91 \text{ \AA}$  and  $r_{\text{Nb-Nb}} = 2.94 \text{ \AA}$ . All of the three partials were expressed within the first coordination shell which peaked at 2.9 Å and extended up to 3.9 Å. The similarity in the contributions of both species into the first shell might be attributed to their comparable covalent radii. Average coordination of both species by Cr and Nb atoms was approximately 3 and 12, respectively and this feature suggested that the two elements tended to bond very similarly. In fact, in accordance with the amorphous phase, cubic and hexagonal Cr<sub>2</sub>Nb phases have been known

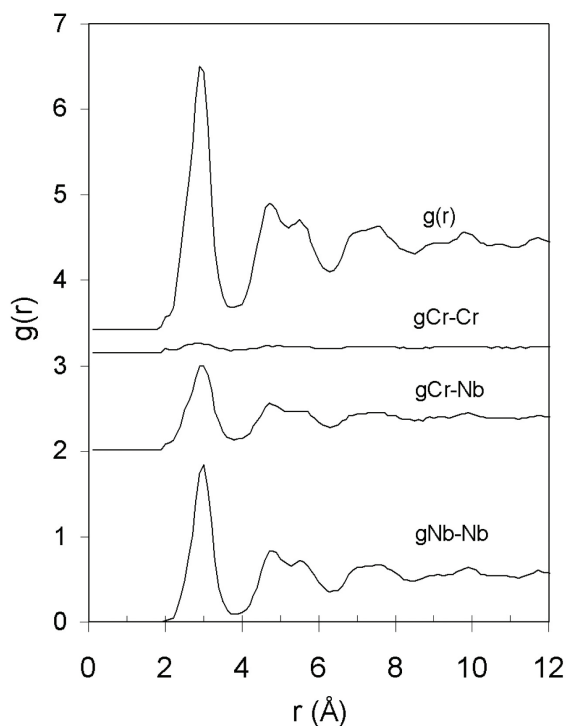


**Figure 1.** Total and partial pair distribution functions calculated in the current study on the basis of the RMC supercell derived in<sup>6</sup>.

to have six closest neighbours at interatomic distances of 2.89 Å; it is thus possible that, e.g., distorted such polyhedra may provide the basis of Cr-Nb contributions into the first coordination peak upon cooling from the melt. Hence, the structure is characteristically dense.

#### 3.2. Atomic environment statistics

Histograms of atom coordination number, cluster number density and cluster mass density of atoms in the first coordination shell are shown in Figure 2. Average coordination of the Cr and Nb species was 12.571 and 12.705, respectively (see Figure 2a). A feature that raised interest was regarding the shapes of both Figures 2b and 2c which were suggestive of binomial or binomial-like distributions. More specifically, cluster number density (Figure 2b) appeared to be centered on two distinct peaks, of 0.05 and 0.06 atoms/Å<sup>3</sup>. The same feature was valid for the Nb distribution, which was centered on 0.06 and 0.07 atoms/Å<sup>3</sup>. The indication of a binomial trend was more pronounced in the case of cluster density (Figure 2c); Both Cr and Nb could be argued as comprising two overlapping distributions, peaking at 8 and 9 g/ml, respectively. In fact, this trend was also noticeable in Figure 2a, where two separate peaks, at 13 and 14, might be tentatively assigned to Cr. Nb coordination distribution, on the other hand, did not appear as decidedly binomial. The feature of binomially distributed atomic environment statistics was also evident in our previous work on bulk metallic glasses<sup>7,8,15</sup>.

Cluster radial distributions were constructed by first considering each of the Cr and Nb centers surrounded by first coordination shell atoms. Then, each center's average

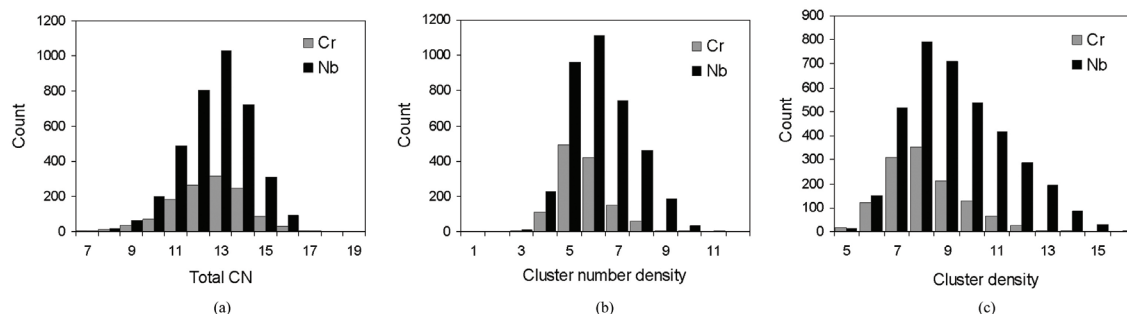


**Figure 2.** Particle histograms (i.e. number of particles in each histogram bin vs. a) coordination number, CN, b) cluster number density and c) mass density) within the second coordination shell of interatomic interactions. The cluster number density values must be multiplied by 0.01 to yield units of atoms/Å<sup>3</sup>. Cluster density is expressed in g/ml.

and partial coordination numbers as well as the cluster's number density and average density were binned based on the metal center's distance from the center of the RMC supercell. The bin values were not normalized by the volume of the spherical shell corresponding to each bin so as to avoid creating a bias towards coordination features close to the RMC box center. As a result, the most intense features were located at distances beyond 10 Å of the RMC box center. The radial variation of metal center coordination number and cluster number density is shown in Figure 3.

### 3.3. Cluster selection

The highest-intensity feature of Cr-centered clusters was found to lie in the region of 20–22 Å and involved average cluster coordinations of between 12 and 14 (see Figure 3a). These moieties also had average number densities in the region of 0.05–0.06 atoms/Å<sup>3</sup> (rounded up to two decimal points – see Figure 3c). Also, as seen in Figure 3b, the Cr clusters in this region were coordinated by roughly two to four Cr surface atoms. Interestingly, Cr surface atom coordination was the same for Nb-centered clusters (see Figure 3e) in spite of the lower content of Cr atoms in the system. This probably serves as an indication of the increased collaboration between Cr–Cr and Cr–Nb. The most intense features of the radial distribution of cluster number density (Figures 3c and 3f) followed suite from coordination and were also observed within the region of 20–22 Å. On the basis of average atomic coordination, average cluster number density and of the radial distribution of these quantities we selected a number of clusters as representative of the RMC supercell.

Details of the selected clusters are listed in Table 1. The BLYP/TZ2P lowest energy state of each of the clusters selected was determined as the most negative value from the plot of cluster binding energy vs. spin polarization, while cluster charges varied in the range of –1 to 1.

### 3.4. Cluster relaxation

The variation of cluster binding energy over a wide polarization range (0 to 15) is shown in Figure 4. Cluster relaxation under charge neutrality did not, generally, yield the lowest of the energy states. In our previous studies of covalent glasses it was shown that the ground state of isolated metallic clusters was best described by negatively

charged moieties of rather high spin multiplicities (typically up to 12)<sup>7,8,15</sup>. A review of Figure 4 confirms that this is also true for the Cr<sub>25</sub>Nb<sub>75</sub> system. More precisely, cluster ground states were always associated with a formal charge of –1 and spin compensations that ranged from 6 to 15. For the sake of completeness we have opted to report on both the negatively charged as well as the charge neutral moieties for each cluster. In both the charged and charge neutral geometries, the difference in stereochemistry between the most cohesive and the least cohesive clusters (designated as Cr922 and Nb4961, respectively) was due to the same feature: transition from Cr922 to Nb4961 involved a decrease in Cr coordination (from 3 to 2) and an increase in Nb coordination (from 9 to 11) of the metal centers and this coordination shift was instrumental to cluster stability in a wider context.

To illustrate this further for the case of charged and charge neutral lowest energy states respectively, we introduce the plots of cluster binding energy vs. cluster density (Figures 5a and 5d) and cluster binding energy vs. cluster center coordination (Figures 5b and 5e). Cluster binding energy generally increased with increasing cluster density and one would expect that, given the species' similarity in their coordination requirements, this feature would be owing to both the Cr and Nb centers. However, this was not the case. Increased cluster cohesion was mediated exclusively by the solute-centered clusters upon increase of the number of coordinated atoms regardless of species; Nb-centered clusters appeared to behave in exactly the opposite manner and this solute-solvent competitive effect was in accordance with our own previous observations regarding Ge–Se glass clusters<sup>8</sup>.

### 3.5. Cluster energy decomposition and molecular orbital interactions

Cluster binding energy decomposition into its constituent Pauli, electrostatic and orbital interaction parts is presented in Figures 5c and 5f for the case of charged and charged neutral clusters. Binding energy values corresponding to Figures 5c and 5f are listed in Table 2. From the graphs some consistent observations can be made, focusing on coarse-grained qualitative characteristics. Cluster stability (based on binding energy) was largely the same for both charges.

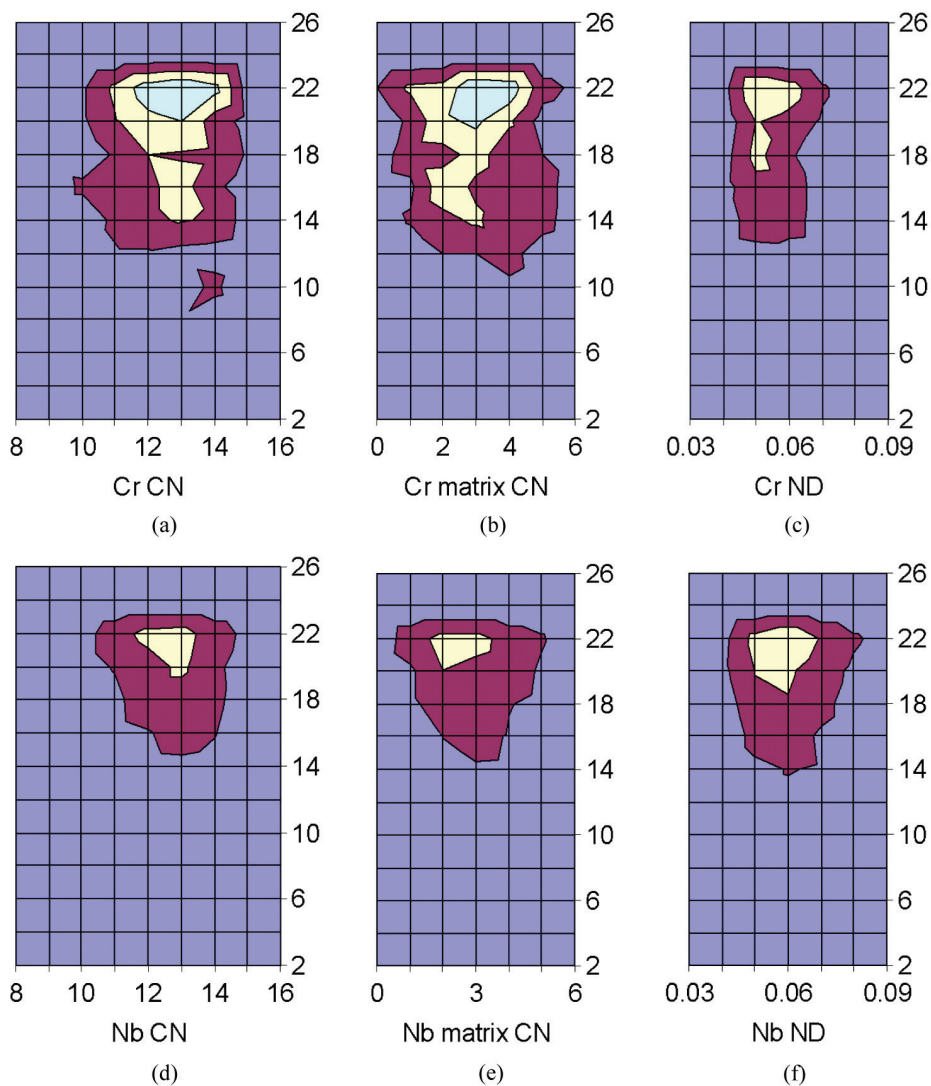


**Figure 3.** Surface plots of the radial distribution of coordination and number density for Cr- and Nb- centered clusters (the radial direction is measured from the origin of the RMC simulation box and is the vertical axis in units of Å). Panels (a) and (d) depict cluster average coordination, (b) and (e) portray cluster coordination by the matrix element, while (c) and (f) represent the variation of cluster number density for Cr- and Nb-centered clusters, respectively. Horizontal axis notation is as follows: CN: average coordination number, matrix CN: average coordination of the cluster center by Cr ('matrix' refers to the first atomic species in the chemical formula, i.e. Cr, by convention), ND: number density (atoms/Å<sup>3</sup>) and D: density (g/ml).

**Table 1.** A list of the most characteristic clusters of the Cr<sub>25</sub>Nb<sub>75</sub> system selected on the basis of the radial distributions of cluster center average coordination, cluster center coordination by the matrix species (conventionally taken to be the first element appearing in the formula unit, i.e. Cr) and cluster number density.

Cluster designation	Center atom	Average coordination of cluster center	Cluster density (g/ml)	Cluster number density (Atoms/Å <sup>3</sup> )	Number of Cr surface atoms	Number of Nb surface atoms
Cr922	Cr	12	11.254460	0.084381	3	9
Cr1167	Cr	13	10.104280	0.074919	3	10
Nb4420	Nb	13	14.173820	0.101443	3	10
Cr915	Cr	12	8.871543	0.069227	4	8
Nb3905	Nb	12	11.483870	0.082855	3	9
Cr726	Cr	14	9.550293	0.070138	4	10
Cr868	Cr	14	11.331020	0.086079	4	10
Cr951	Cr	13	7.421946	0.057084	4	9
Nb4929	Nb	12	11.584020	0.080541	2	10
Nb4961	Nb	13	10.841170	0.074987	2	11

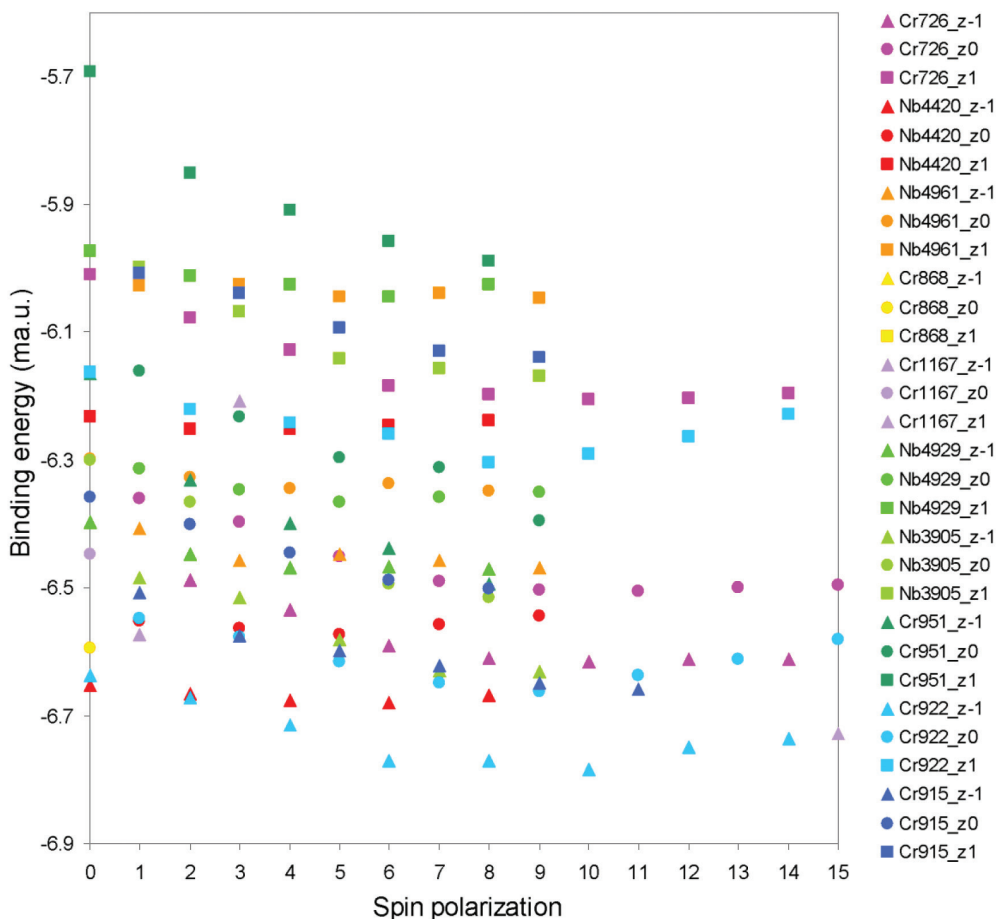


**Figure 4.** Variation of cluster binding energy vs. spin polarization for the clusters listed in Table 2. Legend notation is as follows: cluster name (corresponding to the designation listed in Table 2) followed by the cluster's formal charge; the later is represented by the letter 'z' and either of -1, 0 or 1, for negatively charged, charge neutral and positively charged clusters, respectively.

**Table 2.** Cluster spin polarization, number of electrons,  $N_e$ , and binding energy decomposition.

Cluster designation	Cluster charge	Cluster spin polarization	Ne	Pauli (a.u.)	Electrostatic (a.u.)	Orbital Interactions (a.u.)
Cr922 z-1 s10	-1	10	466	14.469	-7.018	-14.236
Cr1167 z-1 s15	-1	15	507	15.445	-7.436	-14.736
Nb4420 z-1 s6	-1	6	524	19.938	-9.438	-17.178
Cr915 z-1 s11	-1	11	449	12.591	-6.163	-13.086
Nb3905 z-1 s9	-1	9	483	16.369	-7.834	-15.165
Cr726 z-1 s10	-1	10	548	12.713	-6.200	-13.129
Cr868 z0 s0	0	0	530	16.310	-7.803	-15.101
Cr951 z-1 s8	-1	8	490	11.457	-5.588	-12.361
Nb4929 z-1 s8	-1	8	500	15.760	-7.604	-14.626
Nb4961 z-1 s9	-1	9	541	15.397	-7.461	-14.404
Cr922 z0 s9	0	9	466	14.469	-7.018	-14.114
Cr868 z0 s0	0	0	530	16.310	-7.803	-15.101
Nb4420 z0 s5	0	5	524	19.938	-9.438	-17.072
Nb3905 z0 s8	0	8	483	16.369	-7.834	-15.049
Cr726 z0 s11	0	11	548	12.713	-6.200	-13.017
Cr915 z0 s8	0	8	449	12.591	-6.163	-12.930
Cr1167 z0 s0	0	0	507	15.445	-7.436	-14.456
Cr951 z0 s9	0	9	490	11.457	-5.588	-12.263
Nb4929 z0 s5	0	5	500	15.760	-7.604	-14.521
Nb4961 z0 s8	0	8	541	15.397	-7.461	-14.285

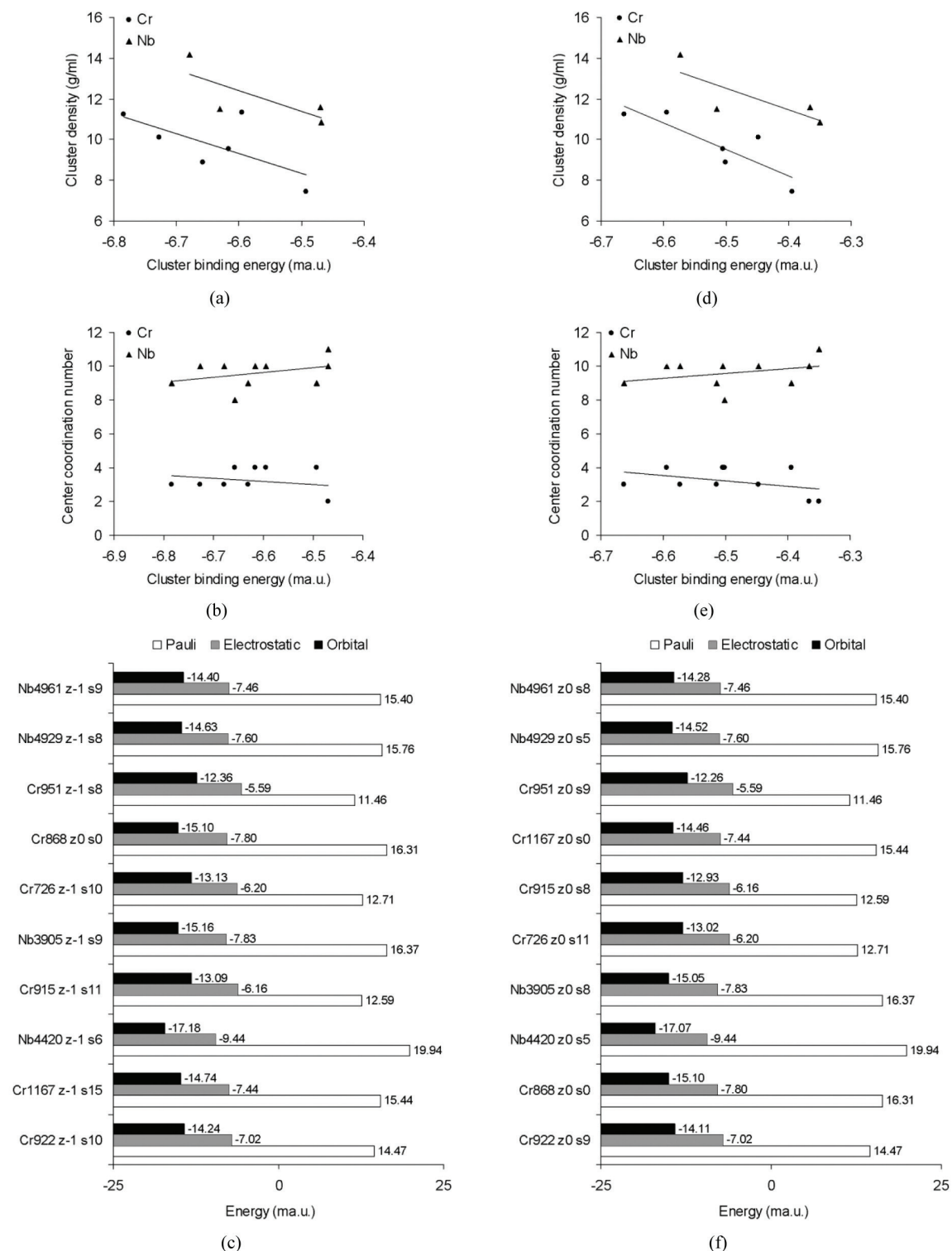


**Figure 5.** Cluster binding energy vs. cluster density (a and d) and cluster center coordination (b and e) as well as decomposition of cluster binding energy (c and f). Panels on the left column represent cluster ground states (found mostly at a cluster formal charge of -1) while panels on the right column represent cluster lowest energy states at charge neutrality. Both columns represent the lowest energy states found over a wide range of spin polarization (between 0 and 15). The sequence of clusters in panels (c) and (f) is in ascending negative energy order (thus, clusters Nb4961 and Cr922 are the least cohesive and most cohesive, respectively). Cluster notation: cluster name, then the letter 'z' and the cluster's charge followed by the letter 's' and the cluster's spin polarization.



**Figure 6.** Valence atomic orbital contributions as a percentage of total molecular orbital density for the clusters under study. The first and second columns respectively represent the majority (spin up) and minority (spin down) populations of the cluster ground state at any combination of charge and spin polarization. Similarly, the third and fourth columns represent majority and minority populations of cluster lowest energy states at charge neutrality. In all columns, the vertical sequence of the clusters follows from Figure 5. Colour notation is as follows:  $\text{Cr-t}_{2g}$  – blue,  $\text{Cr-e}_g$  – dark red,  $\text{Nb-t}_{2g}$  – light yellow and  $\text{Nb-e}_g$  – cyan.

Principal features of cluster stability were a) an inverse relationship between Pauli repulsion and electrostatic interactions and b) a covariance between and electrostatic and orbital interactions. Atomic orbital  $t_{2g}$  and  $e_g$  contributions for the most representative clusters under study are shown in Figure 6, as percentages of total molecular orbital (MO) density. MO's were dominated by Nb contributions, regardless of cluster spin and charge. Spin polarized moieties also exhibited pronounced spin mixing between the Cr and Nb states.

A rather interesting additional feature was the similarity of valence populations in both the lowest energy charged and charge neutral cases, a fact also confirmed by the similarity in molecular orbital-related energies in Figures 5c and 5f. Therefore, a side-by-side comparison of the charged and charge neutral moieties of Figure 6 would not offer insight towards the fundamentals of cluster stability. However, both charge states showed common features, beginning with increased contributions of Nb- $t_{2g}$  populations which transcended cluster stability over the whole spectrum of binding energies shown. Moreover, Nb- $e_g$  cooperation with Nb- $t_{2g}$  was always intense in both spins.

Cr majority population contributions were also high (typically 30% of the MO density) across the range of clusters studies, reaching up to 80% of MO density in certain instances; however, there was no detectable trend between MO energy, Cr  $\alpha$ -spin contributions and cluster stability. However, a relation between cluster stability and  $\beta$ -spin Cr populations, particularly of Cr- $e_g$  character, might exist. As shown in Figure 6, a comparison of minority populations, e.g. between the least and most stable clusters (Nb4961 and Cr922 respectively) reveals that in the latter MO interactions between valence states of both atomic species are more pronounced, particularly in energies below  $-0.15$  a.u.

## References

1. Nagase T, Ueda M and Umakoshi Y. Preparation of Ni-Nb-based metallic glass wires by arc-melt-type melt-extraction method. *Journal of Alloys and Compounds*. 2009; 485(1-2):304-312. <http://dx.doi.org/10.1016/j.jallcom.2009.05.122>.
2. Castro JFR, Santos SF, Ishikawa T and Botta WJ. Processing and microstructural characterization of a Ti-Cr-Nb alloy synthesized by high-energy ball-milling. *Materials Research*. 2012; 15(5):753-756. <http://dx.doi.org/10.1590/S1516-14392012005000061>.
3. Thoma DJ, Perepezko JH, Plantz DH and Schwarz RB. Metastable b.c.c. phase formation in the Nb-Cr system. *Materials Science and Engineering A*. 1994; 179-180:176-180. [http://dx.doi.org/10.1016/0921-5093\(94\)90188-0](http://dx.doi.org/10.1016/0921-5093(94)90188-0).
4. Takeyama M and Liu CT. Microstructure and mechanical properties of Laves-phase alloys based on Cr2Nb. *Materials Science and Engineering A*. 1991; 132(0):61-66. [http://dx.doi.org/10.1016/0921-5093\(91\)90361-P](http://dx.doi.org/10.1016/0921-5093(91)90361-P).
5. Goldschmidt HJ and Brand JA. The constitution of the chromium-niobium-molybdenum system. *Journal of the Less Common Metals*. 1961; 3(1):44-61. [http://dx.doi.org/10.1016/0022-5088\(61\)90042-X](http://dx.doi.org/10.1016/0022-5088(61)90042-X).
6. Lima JC, Almeida TO, Jerônimo AR, Souza SM, Campos CEM and Grandi TA. Reverse Monte Carlo simulations of an amorphous Cr25Nb75 alloy produced by mechanical alloying.

## 4. Conclusions

The short range order of a mechanically alloyed Cr<sub>25</sub>Nb<sub>75</sub> glass was determined by DFT analysis of representative clusters, isolated from an RMC supercell on the basis of atomic environment statistics. According to the results obtained, the following conclusions could be drawn:

1. Average coordination of both Cr and Nb atoms was very similar which, coupled with the similarity of their covalent radii, suggested uniformity in covalent bonding between the two.
2. The histograms of average elemental coordination and average cluster density for both atomic species revealed a tendency for binomial distributions. The latter may reflect two separate modes of atomic bonding or may be a systematic bias of the RMC fitting. More work needs to be carried out to account for this effect.
3. Cluster stability was characterized by a) an inverse relationship between Pauli repulsion and electrostatic interactions and b) a covariance between and electrostatic and orbital interactions. Also, cluster cohesion was affected by solute-solvent interactions. More precisely, Cr centers were more stable than Nb centers and their stability increased with coordination.
4. A tentative case was made for the existence of a relation between cluster stability and minority Cr populations.

## Acknowledgements

The provision of the RMC configuration files by Dr J.C. de Lima is gratefully acknowledged.

- Journal of Non-Crystalline Solids*. 2006; 352(2):109-115. <http://dx.doi.org/10.1016/j.jnoncrysol.2005.11.020>.
7. Antipas GSE. Molecular orbital interactions in glass-forming Zr70Cu30 liquid quasicrystals. *Journal of Alloys and Compounds*. 2013; 578:565-570. <http://dx.doi.org/10.1016/j.jallcom.2013.06.179>.
  8. Antipas GSE, Mangiorou E and Hristoforou E. Solute-solvent interactions and atomic cohesion in GeSe4 and GeSe4In5 metallic glasses. *Materials Research Express*. 2014; 1(1):015202. <http://dx.doi.org/10.1088/2053-1591/1/1/015202>.
  9. Becke AD. Density-functional exchange-energy approximation with correct asymptotic behavior. *Physical Review A*. 1988; 38(6):3098-3100. <http://dx.doi.org/10.1103/PhysRevA.38.3098>. PMID:9900728
  10. Lee C, Yang W and Parr RG. Development of the Colle-Salvetti correlation-energy formula into a functional of the electron density. *Physical Review B: Condensed Matter and Materials Physics*. 1988; 37(2):785-789. <http://dx.doi.org/10.1103/PhysRevB.37.785>. PMID:9944570
  11. van Lenthe E, Baerends EJ and Snijders JG. Relativistic total energy using regular approximations. *The Journal of Chemical Physics*. 1994; 101(11):9783-9792. <http://dx.doi.org/10.1063/1.467943>.
  12. Belanzoni P, van Lenthe E and Baerends EJ. An evaluation of the density functional approach in the zero order regular approximation for relativistic effects: Magnetic interactions



- in small metal compounds. *The Journal of Chemical Physics*. 2001; 114(10):4421. <http://dx.doi.org/10.1063/1.1345509>.
13. Van Lenthe E, van der Avoird A and Wormer PES. Density functional calculations of molecular hyperfine interactions in the zero order regular approximation for relativistic effects. *The Journal of Chemical Physics*. 1998; 108(12):4783. <http://dx.doi.org/10.1063/1.475889>.
  14. Scientific Computing & Modelling – SCM. *Amsterdam Density Functional program. Theoretical Chemistry*. Amsterdam: Vrije Universiteit; 2010.
  15. Antipas GSE and Mangiorou E. Atomic topology and electronic structure of a melt-spun Al92U8 metallic glass. *Computational and Theoretical Chemistry*. 2014; 1036:16-21. <http://dx.doi.org/10.1016/j.comptc.2014.03.009>.